Lithium Ion Batteries

Deutsche Ausgabe: DOI: 10.1002/ange.201600133
Internationale Ausgabe: DOI: 10.1002/anie.201600133

Hierarchical Tubular Structures Composed of Co_3O_4 Hollow Nanoparticles and Carbon Nanotubes for Lithium Storage

*Yu Ming Chen, Le Yu, and Xiong Wen (David) Lou**

Abstract: *Hierarchical tubular structures composed of Co_3O_4 hollow nanoparticles and carbon nanotubes (CNTs) have been synthesized by an efficient multi-step route. Starting from polymer-cobalt acetate ($Co(Ac)_2$) composite nanofibers, uniform polymer-$Co(Ac)_2$@zeolitic imidazolate framework-67 (ZIF-67) core–shell nanofibers are first synthesized via partial phase transformation with 2-methylimidazole in ethanol. After the selective dissolution of polymer-$Co(Ac)_2$ cores, the resulting ZIF-67 tubular structures can be converted into hierarchical CNTs/Co-carbon hybrids by annealing in Ar/H_2 atmosphere. Finally, the hierarchical CNT/Co_3O_4 microtubes are obtained by a subsequent thermal treatment in air. Impressively, the as-prepared nanocomposite delivers a high reversible capacity of 1281 mAh g^{-1} at 0.1 A g^{-1} with exceptional rate capability and long cycle life over 200 cycles as an anode material for lithium-ion batteries.*

Lithium-ion batteries (LIBs) have been the focus of intensive efforts for portable electronic devices, electric vehicles, and hybrid electric vehicles.[1–6] However, existing commercial graphite based anodes have a relatively low theoretical capacity of 372 mAh g^{-1}, which is far below the specifications required in large-scale energy applications.[7–9] Thus, it is highly desirable to explore alternative anode materials that could endow LIBs with higher energy density and better rate performance. Cobalt oxide based materials have attracted a lot of attention as promising anode materials.[10–13] Of particular note, mixed-valent Co_3O_4 can theoretically deliver as high as three times the capacity of graphite due to its 8-electron transfer reaction upon cycling.[13–19] Unfortunately, the practical applications of Co_3O_4-based electrodes are largely hampered due to the poor electrical conductivity and the large volumetric variation during the charging-discharging processes.[12,13,20,21]

Nanostructured electrode materials can enhance the electrochemical performance that could not be achieved in traditional bulk materials, benefiting from the higher surface area and shorter diffusion path.[22–25] Amongst various structural designs, considerable attention has been paid to hierarchical tubular structures (HTSs) in view of their many advantages such as enlarged electrode/electrolyte contact area and pore volume. These hierarchical microtubes are usually organized by low-dimensional building blocks. For instance, Wang and co-workers reported a simple solution-phase method for constructing robust tubular structure composed of single-layered MoS_2 for lithium storage.[26] Our group has also synthesized several hierarchical tubulars constructed from Mn-based mixed metal oxide nanoflakes and TiO_2 (B) nanosheets by efficient template-based strategies as advanced electrode materials.[27,28] More recently, great efforts have been devoted to designing hybrid nanostructures of inorganic nanostructures and carbon-based species for LIBs application. It is generally believed that these hybrid constructions could simultaneously overcome the shortcomings of poor mechanical stability and poor electrical conductivity in simple inorganic materials.[29–32] Despite the progresses, the designed synthesis of HTSs constructed from different types of functional subunits is still quite challenging due to the limitations of synthetic strategies.

Herein, we have designed a multi-step strategy for the efficient synthesis of novel HTSs composed of Co_3O_4 hollow nanoparticles and carbon nanotubes (CNTs). Through a controlled chemical transformation process, zeolitic imidazolate framework-67 (ZIF-67) tubulars have been made as the single source for carbon and cobalt in the final composite. After a two-step annealing treatment, the hierarchical CNT/Co_3O_4 microtubes are obtained, which inherit unique structural features from the different functional subunits. Specifically, these HTSs constructed by hollow nanoparticles can provide sufficient active interfacial sites and effectively alleviate the volume variation during the electrochemical reactions. The well-distributed CNTs on the HTSs ensure the enhanced electron transfer and prevent the aggregation of Co_3O_4 nanoparticles during cycling processes. As expected, the as-prepared hierarchical CNT/Co_3O_4 microtubes show excellent electrochemical properties as an anode material for LIBs.

The synthesis process of the hierarchical CNT/Co_3O_4 microtubes involves the following steps as schematically shown in Figure 1. Electrospun polyacrylonitrile (PAN)–cobalt acetate ($Co(Ac)_2$) composite nanofibers are selected as the self-engaged templates to provide the cobalt source for the growth of ZIF-67. Next, due to the strong coordination of 2-methylimidazole to cobalt ions within the PAN–$Co(Ac)_2$ nanofibers, a uniform shell of ZIF-67 nanocrystals can be grown on the nanofibers. After being dispersed in *N*,*N*-dimethylformamide (DMF) to dissolve the PAN–$Co(Ac)_2$ core, the obtained ZIF-67 tubulars can be further converted into CNT/Co–carbon hybrids through a heating treatment in Ar/H_2. During this process, elemental Co nanoparticles are first yielded in the strong reduction atmosphere. At the same time, the highly dispersed Co nanoparticles can catalyze the

[*] Dr. Y. M. Chen, Dr. L. Yu, Prof. X. W. Lou
School of Chemical and Biomedical Engineering
Nanyang Technological University
62 Nanyang Drive, Singapore 637459 (Singapore)
E-mail: xwlou@ntu.edu.sg
Homepage: http://www.ntu.edu.sg/home/xwlou/

Supporting information for this article can be found under: http://dx.doi.org/10.1002/anie.201600133.

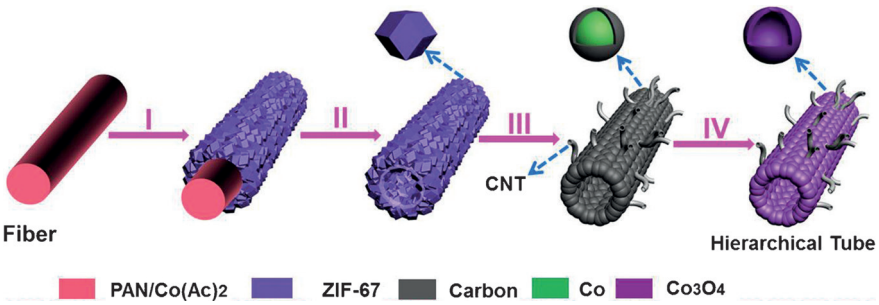

Figure 1. Formation of the hierarchical CNT/Co_3O_4 microtubes. I) The growth of ZIF-67 onto the PAN–$Co(Ac)_2$ composite nanofiber. II) Removal of the PAN–$Co(Ac)_2$ core. III) Heating treatment in Ar/H_2 to convert ZIF-67 tubular structures to hierarchical CNT/Co-carbon composites. IV) Further calcination in air to obtain hierarchical CNT/Co_3O_4 microtubes.

growth of CNTs from carbon precursor,[33–35] leading to the formation of the hierarchical hybrids. Finally, these Co nanoparticles are oxidized to Co_3O_4 hollow nanoparticles via a thermal annealing in air while the CNTs can be well retained, generating hierarchical CNT/Co_3O_4 microtubes.

$Co(Ac)_2$ can be uniformly distributed in the PAN nanofibers to form the PAN-$Co(Ac)_2$ composite nanofibers by an electrospinning method (Figure S1 a–c, see Supporting Information), as confirmed by energy-dispersive spectroscopy (EDX) spectrum (Figure S1 d). The typical field-emission scanning electron microscopy (FESEM) images (Figure S2 a–c) show that 2-methylimidazole can react with $Co(Ac)_2$ in the composite nanofibers to generate ZIF-67 nanocrystals. Transmission electron microscopy (TEM) images clearly reveal a core–shell structure (Figure S2 d–f). XRD pattern of the composites indicates typical diffraction peaks of ZIF-67 phase (Figure S3a).[36,37] As elucidated in Figure 2, the PAN-$Co(Ac)_2$ core is completely removed after the treatment in DMF. The remaining ZIF-67 nanocrystals are interconnected to build tubular structures. In addition, the ZIF-67 particle size is about 40 to 80 nm, which can be slightly reduced using methanol as the solvent (Figure S4). When annealed in Ar/H_2 atmosphere, the as-synthesized ZIF-67 microtubes can be transformed into the CNT/Co–carbon hybrids. Some multiwalled CNTs can be clearly identified on the surface of Co–carbon composite (Figure S5). The interplanar spacings of 0.34 nm and 0.21 nm correspond to the (002) planes of carbon and the (111) planes of Co, respectively. Selected area electron diffraction (SAED) pattern (Figure S5 c) and XRD pattern (Figure S3 b) further confirm the presence of elemental Co.

In the final step, a mild annealing treatment at 360 °C in air is employed to convert the CNT/Co–carbon composites into the hierarchical CNT/Co_3O_4 microtubes. The tubular morphology of the materials is well maintained after the oxidation process (Figure 3, and Figure S6). More interestingly, the tubulars are mainly organized by Co_3O_4 hollow nanoparticles with a size ranged from 15 to 30 nm (Figure 3 c–e). The transformation from Co solid nanoparticles into Co_3O_4 hollow particles can be attributed to the Kirkendall effect during the annealing process.[38,39] Moreover, CNTs can be generally retained after the calcination in air, yielding hierarchical CNT/Co_3O_4 microtubes (Figure 3 b,d). In addition, the inner diameter of Co_3O_4 hollow nanoparticle and CNTs is about 10 ± 5 nm and 3 ± 2 nm, respectively (Figure 3 d–f). The clear lattice fringes with an interplanar distance of 0.24 nm can be ascribed to the (311) planes of the cubic Co_3O_4 (Figure 3 e). The crystallographic structure of the microtubes are then investigated by XRD (Figure S3 b). All the diffraction peaks can be perfectly indexed to cubic Co_3O_4 (JCPDS card No.: 42-1467), which is consistent with the high-resolution TEM (HRTEM) image and selected area electron diffraction (SAED) analysis (Figure 3 e and Figure S6 c). EDX analysis reveals that the Co/O atomic ratio of the microtubes is about 0.79 (Figure S7). As verified by thermogravimetric analysis (TGA; Figure S8), the carbon content in the composite is about 13 %. The X-ray photoelectron spectroscopy (XPS) spectrum confirms the existence of pyridinic N (398.5 eV) and pyrrolic N (400.8 eV) in the composites (Figure S9). Moreover, the hierarchical CNT/Co_3O_4 microtubes exhibit a high specific Brunauer–Emmett–Teller (BET) surface area of 93.9 $m^2 g^{-1}$ with the pore sizes mostly below 15 nm (Figure S10). It is worth to mention that the selection of the atmosphere and temperature in the two-step annealing treatment plays important roles in the generation of the unique hierarchical structures. If Ar is used instead of Ar/H_2 in the first-step of annealing treatment, only Co_3O_4 microtubes could be achieved without the formation of CNTs (Figure S11). When a lower calcining temperature is applied in the oxidization step, significant amount of residual carbon will remain in the final materials (Figure S7 b and S12).

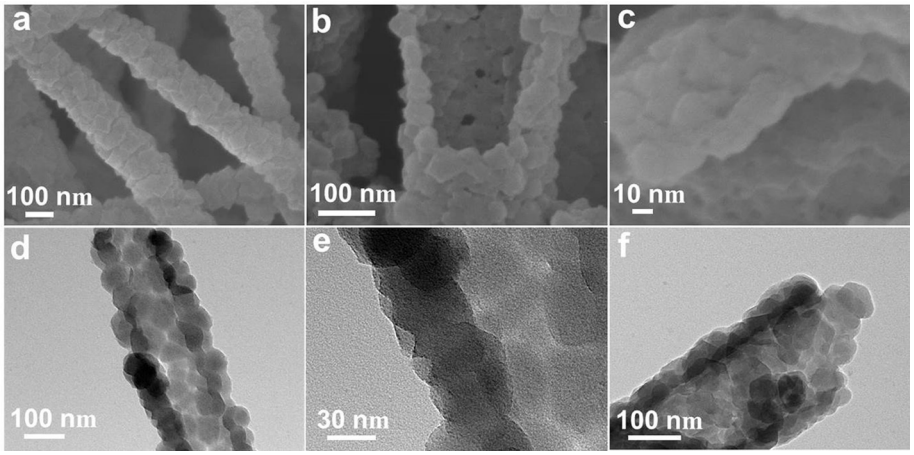

Figure 2. a–c) FESEM and d–f) TEM images of the synthesized ZIF-67 microtubes.

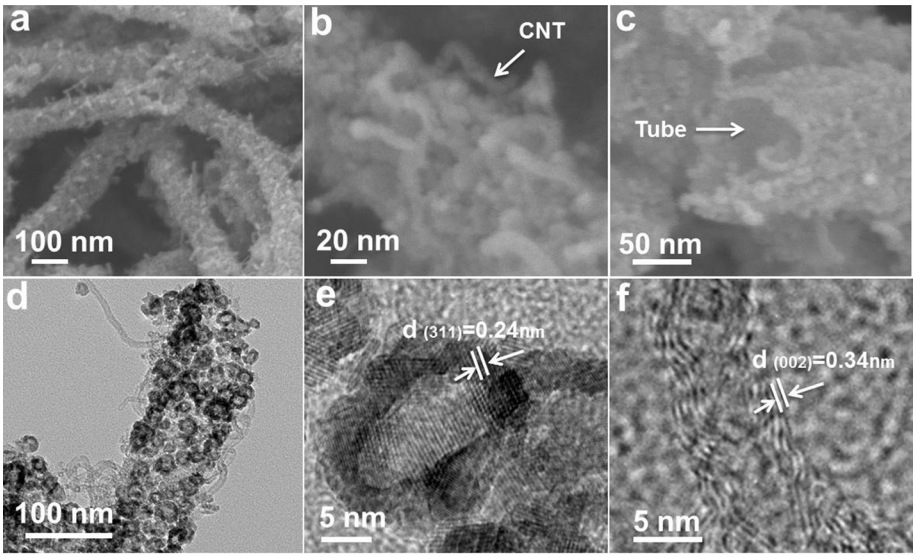

Figure 3. a–c) FESEM, d) TEM, and e,f) HRTEM images of the synthesized hierarchical CNT/Co_3O_4 microtubes.

Figure 4a presents the typical galvanostatic charge-discharge voltage profiles of the hierarchical microtubes at the current density of 0.1 Ag^{-1}. A long voltage plateau at around 1.03 V and the other inconspicuous plateau at about 1.3 V can be observed in the first discharge process, corresponding to the reduction reactions of CoO to Co and Co_3O_4 to CoO, respectively.[40] The main plateau at 2.1 V can be assigned to the delithiation of Co to Co_3O_4 in the first charge process.[16] The voltage plateau obviously shifts to about 1.25 V in the second discharge cycle, which could be mainly attributed to the structural variation of the electrode materials.[20,40] Nevertheless, the voltage profiles are well overlapping except for the initial discharge, indicating the good stability of the composites for reversible lithium storage. The representative cyclic voltammetry (CV) curves of these hierarchical microtubes further confirm the typical multi-step electrochemical processes of Co_3O_4 (Figure S13). The first charge and discharge specific capacities are about 1281 and 1840 mAh g^{-1}, respectively, which are much higher than those of the CNTs derived from the hierarchical CNT/Co_3O_4 microtubes after acid treatment (Figure S14). The relatively large irreversible capacity could be due to the formation of the solid-electrolyte interface (SEI) film and the decomposition of electrolyte.[14,17,41]

The rate capability of the CNT/Co_3O_4 electrode is shown in Figure 4b. At current densities of 0.75, 1.25, 2, 2.5, and 3 A g^{-1}, the reversible capacities of the hierarchical microtubes are around 832, 768, 715, 673, and 643 mAh g^{-1}, respectively. Even at a relatively high current density of 6 A g^{-1}, the hierarchical hybrid can still deliver a capacity as high as 515 mAh g^{-1}. The capacity is slightly increased during the cycling process when the current density is decreased to 0.75 A g^{-1}, due to the reactivation process caused by the high-rate lithiation.[42] More importantly, the hierarchical CNT/Co_3O_4 electrode also exhibits exceptional cycling stability. As shown in Figure 4c, the as-prepared electrode shows a high capacity of 782 and 577 mAh g^{-1} after 200 cycles at 1 and 4 A g^{-1}, respectively, without obvious capacity fading. The Coulombic efficiency (CE) for the CNT/Co_3O_4 composite electrode is close to 100% after the first few cycles. This performance is superior to that of many other Co_3O_4-based anodes (Table S1). Post-mortem study shows that the shape and structural integrity of the CNT/Co_3O_4 composite can be well retained after 200 cycles (Figure S15). The outstanding performance of the hierarchical CNT/Co_3O_4 microtubes might be attributed to the unique structural and compositional features. To be specific, the construction of Co_3O_4 hollow nanoparticle and CNT subunits not only enables a short diffusion distance for fast diffusion of

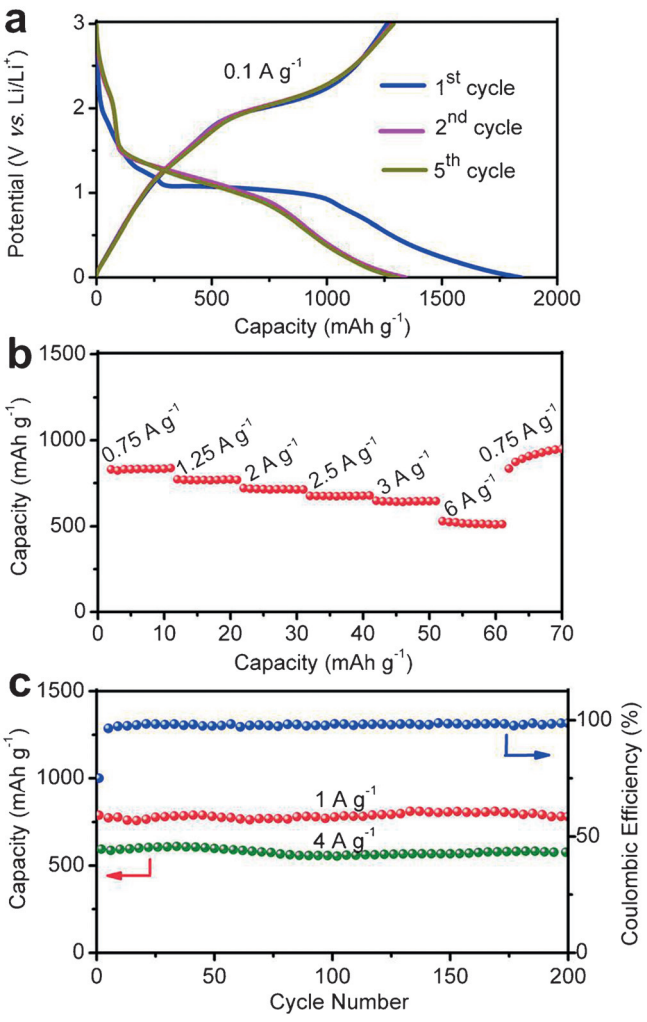

Figure 4. Electrochemical performance of the hierarchical CNT/Co_3O_4 microtubes. a) Charge–discharge voltage profiles at 0.1 A g^{-1}, b) rate performance, and c) cycling performance and Coulombic efficiency.

Li^+ ions but also provides sufficient contact between active material and electrolyte for the rapid charge-transfer reaction.[20] Moreover, the tubular structures and void space within the Co_3O_4 nanoparticles can effectively withstand large volume variation upon cycling, therefore maintaining structural integrity.[40] In addition, the CNTs integrated in the hierarchical tubulars can enhance the electronic conductivity thus improving the rate capability,[34,43] as well as the electrochemical reactivity further improving the electrochemical property.[34]

In summary, we have developed a multi-step method for the effective synthesis of hierarchical tubular structures composed of Co_3O_4 hollow nanoparticles and carbon nanotubes (CNTs). Electrospun polyacrylonitrile (PAN)–cobalt acetate ($Co(Ac)_2$) composite nanofibers are used as the bifunctional template. Through a facile chemical transformation process and subsequent removal of the core, tubular-like structures of ZIF-67 nanocrystals are obtained. A two-step annealing process is applied to convert these ZIF-67 tubulars into hierarchical CNT/Co_3O_4 microtubes. Benefiting from the unique structural and compositional advantages, the as-prepared hierarchical CNT/Co_3O_4 tubular structures show excellent electrochemical performance as an anode material for lithium-ion batteries.

Acknowledgements

We thank the Ministry of Education (Singapore) for financial support through the AcRF Tier 2 funding (MOE2014-T2-1-058, ARC41/14; M4020223.120).

Keywords: Co_3O_4 · hierarchical microtubes · hollow nanoparticles · lithium-ion batteries · ZIF-67

How to cite: *Angew. Chem. Int. Ed.* **2016**, *55*, 5990–5993
Angew. Chem. **2016**, *128*, 6094–6097

[1] M. Armand, J. M. Tarascon, *Nature* **2008**, *451*, 652.
[2] K. S. Kang, Y. S. Meng, J. Breger, C. P. Grey, G. Ceder, *Science* **2006**, *311*, 977.
[3] Y. Idota, T. Kubota, A. Matsufuji, Y. Maekawa, T. Miyasaka, *Science* **1997**, *276*, 1395.
[4] A. Kushima, X. H. Liu, G. Zhu, Z. L. Wang, J. Y. Huang, J. Li, *Nano Lett.* **2011**, *11*, 4535.
[5] H. Jiang, D. Ren, H. Wang, Y. Hu, S. Guo, H. Yuan, P. Hu, L. Zhang, C. Li, *Adv. Mater.* **2015**, *27*, 3687.
[6] H. Geng, Q. Zhou, Y. Pan, H. Gu, J. Zheng, *Nanoscale* **2014**, *6*, 3889.
[7] Y. M. Chen, Z. G. Lu, L. M. Zhou, Y. W. Mai, H. T. Huang, *Energy Environ. Sci.* **2012**, *5*, 7898.
[8] K. Sato, M. Noguchi, A. Demachi, N. Oki, M. Endo, *Science* **1994**, *264*, 556.
[9] Z.-J. Fan, J. Yan, T. Wei, G.-Q. Ning, L.-J. Zhi, J.-C. Liu, D.-X. Cao, G.-L. Wang, F. Wei, *ACS Nano* **2011**, *5*, 2787.
[10] Y. Sun, X. Hu, W. Luo, Y. Huang, *J. Phys. Chem. C* **2012**, *116*, 20794.
[11] X. Guan, J. Nai, Y. Zhang, P. Wang, J. Yang, L. Zheng, J. Zhang, L. Guo, *Chem. Mater.* **2014**, *26*, 5958.
[12] D. Gu, W. Li, F. Wang, H. Bongard, B. Spliethoff, W. Schmidt, C. Weidenthaler, Y. Xia, D. Zhao, F. Schüth, *Angew. Chem. Int. Ed.* **2015**, *54*, 7060; *Angew. Chem.* **2015**, *127*, 7166.
[13] J. Wang, N. Yang, H. Tang, Z. Dong, Q. Jin, M. Yang, D. Kisailus, H. Zhao, Z. Tang, D. Wang, *Angew. Chem. Int. Ed.* **2013**, *52*, 6417; *Angew. Chem.* **2013**, *125*, 6545.
[14] R. Tummala, R. K. Guduru, P. S. Mohanty, *J. Power Sources* **2012**, *199*, 270.
[15] W. Wen, J. M. Wu, M. H. Cao, *Nanoscale* **2014**, *6*, 12476.
[16] X. Yang, K. Fan, Y. Zhu, J. Shen, X. Jiang, P. Zhao, S. Luan, C. Li, *ACS Appl. Mater. Interfaces* **2013**, *5*, 997.
[17] Z. S. Wu, W. Ren, L. Wen, L. Gao, J. Zhao, Z. Chen, G. Zhou, F. Li, H. M. Cheng, *ACS Nano* **2010**, *4*, 3187.
[18] D. Qiu, G. Bu, B. Zhao, Z. Lin, L. Pu, L. Pan, Y. Shi, *Mater. Lett.* **2014**, *119*, 12.
[19] B. Wang, X. Y. Lu, Y. Y. Tang, *J. Mater. Chem. A* **2015**, *3*, 9689.
[20] S. Abouali, M. Akbari Garakani, B. Zhang, H. Luo, Z.-L. Xu, J.-Q. Huang, J. Huang, J.-K. Kim, *J. Mater. Chem. A* **2014**, *2*, 16939.
[21] H. Geng, H. Ang, X. Ding, H. Tan, G. Guo, G. Qu, Y. Yang, J. Zheng, Q. Yan, H. Gu, *Nanoscale* **2016**, *8*, 2967.
[22] M. V. Reddy, G. V. Subba Rao, B. V. R. Chowdari, *Chem. Rev.* **2013**, *113*, 5364.
[23] X. Y. Yu, L. Yu, X. W. Lou, *Adv. Energy Mater.* **2016**, *6*, 1501333.
[24] S. Goriparti, E. Miele, F. De Angelis, E. Di Fabrizio, R. Proietti Zaccaria, C. Capiglia, *J. Power Sources* **2014**, *257*, 421.
[25] L. Ji, Z. Lin, M. Alcoutlabi, X. Zhang, *Energy Environ. Sci.* **2011**, *4*, 2682.
[26] P. P. Wang, H. Y. Sun, Y. J. Ji, W. H. Li, X. Wang, *Adv. Mater.* **2014**, *26*, 964.
[27] Y. Guo, L. Yu, C.-Y. Wang, Z. Lin, X. W. Lou, *Adv. Funct. Mater.* **2015**, *25*, 5184.
[28] H. Hu, L. Yu, X. Gao, Z. Lin, X. W. Lou, *Energy Environ. Sci.* **2015**, *8*, 1480.
[29] X. K. Huang, S. M. Cui, J. B. Chang, P. B. Hallac, C. R. Fell, Y. T. Luo, B. Metz, J. W. Jiang, P. T. Hurley, J. H. Chen, *Angew. Chem. Int. Ed.* **2015**, *54*, 1490; *Angew. Chem.* **2015**, *127*, 1510.
[30] X. Y. Yu, H. Hu, Y. W. Wang, H. Y. Chen, X. W. Lou, *Angew. Chem. Int. Ed.* **2015**, *54*, 7395; *Angew. Chem.* **2015**, *127*, 7503.
[31] G. Huang, F. F. Zhang, X. C. Du, Y. L. Qin, D. M. Yin, L. M. Wang, *ACS Nano* **2015**, *9*, 1592.
[32] H. L. Wang, H. J. Dai, *Chem. Soc. Rev.* **2013**, *42*, 3088.
[33] R. Wu, D. P. Wang, X. Rui, B. Liu, K. Zhou, A. W. K. Law, Q. Yan, J. Wei, Z. Chen, *Adv. Mater.* **2015**, *27*, 3038.
[34] Y. M. Chen, X. Y. Li, K. S. Park, J. Song, J. H. Hong, L. M. Zhou, Y. W. Mai, H. T. Huang, J. B. Goodenough, *J. Am. Chem. Soc.* **2013**, *135*, 16280.
[35] B. Y. Xia, Y. Yan, N. Li, H. B. Wu, X. W. Lou, X. Wang, *Nat. Energy* **2016**, *1*, 15006.
[36] H. Hu, B. Y. Guan, B. Y. Xia, X. W. Lou, *J. Am. Chem. Soc.* **2015**, *137*, 5590.
[37] H. Hu, L. Han, M. Z. Yu, Z. Y. Wang, X. W. Lou, *Energy Environ. Sci.* **2016**, *9*, 107.
[38] F. Zhang, C. Yuan, J. Zhu, J. Wang, X. Zhang, X. W. Lou, *Adv. Funct. Mater.* **2013**, *23*, 3909.
[39] Y. D. Yin, R. M. Rioux, C. K. Erdonmez, S. Hughes, G. A. Somorjai, A. P. Alivisatos, *Science* **2004**, *304*, 711.
[40] G. Huang, F. Zhang, X. Du, Y. Qin, D. Yin, L. Wang, *ACS Nano* **2015**, *9*, 1592.
[41] W. Hao, S. Chen, Y. Cai, L. Zhang, Z. Li, S. Zhang, *J. Mater. Chem. A* **2014**, *2*, 13801.
[42] H. Sun, G. Xin, T. Hu, M. Yu, D. Shao, X. Sun, J. Lian, *Nat. Commun.* **2014**, *5*, 4526.
[43] L. Qie, W. M. Chen, Z. H. Wang, Q. G. Shao, X. Li, L. X. Yuan, X. L. Hu, W. X. Zhang, Y. H. Huang, *Adv. Mater.* **2012**, *24*, 2047.

Received: January 6, 2016
Revised: February 18, 2016
Published online: April 5, 2016

